ChemComm

HIGHLIGHT

View Article Online
View Journal | View Issue

Cite this: *Chem. Commun.*, 2024, **60**, 10439

Stereochemistry of natural products from vibrational circular dichroism†

Andrea N. L. Batista,[a] Alessandra L. Valverde,[a] Laurence A. Nafie[b] and João M. Batista Jr*[c]

Secondary metabolites from land and marine (micro)organisms have been at the focus of the drug discovery process for many years. One of the reasons for this success is nature's incredible ability to create intricate molecular scaffolds. Such structural richness, however, makes the structural elucidation, and the absolute configuration assignment in particular, a challenging process. Vibrational circular dichroism (VCD) has emerged as one of the most reliable and versatile methods to unambiguously assign both the absolute configuration and conformations of chiral molecules in solution. Although VCD is no longer a curiosity in the field of molecular spectroscopy after 50 years since its first report, it is still underutilized by natural product chemists worldwide for varying reasons. Herein, we highlight the evolution of the application of VCD to natural product chemistry, focusing on its strengths as well as points that still need improvement. General guidelines for the correct application of VCD to stereochemical studies are also provided.

Received 22nd May 2024,
Accepted 23rd August 2024

DOI: 10.1039/d4cc02481h

rsc.li/chemcomm

Introduction

Special (secondary) metabolites are essential to the effective interaction and adaptation of the resulting organisms to the environment. These compounds are mainly involved in chemical communication, defense, transport, and reproduction.[1] Secondary metabolites are thus endowed with the structural and stereochemical requirements for suitable interaction with their target protein receptors. Such interactions, on the other hand, are not restricted to the receptors they were designed for, which

[a] *Institute of Chemistry, Fluminense Federal University, Outeiro de São João Batista s/n, 24020-141, Niterói-RJ, Brazil*
[b] *Department of Chemistry, 1-014CST, Syracuse University, 13244-4100, Syracuse-NY, USA*
[c] *Federal University of São Paulo, Institute of Science and Technology, R. Talim 330, 12231-280, São José dos Campos-SP, Brazil. E-mail: batista.junior@unifesp.br*

† Electronic supplementary information (ESI) available. See DOI: https://doi.org/10.1039/d4cc02481h

Andrea N. L. Batista

Andrea Batista is a Visiting Researcher in the Institute of Chemistry at Fluminense Federal University, Brazil. She received a BSc in Pharmacy-Biochemistry (1999) from UNESP, Brazil, and a MSc (2001) and PhD (2005) degrees in Chemistry from the same university, supervised by Professor Massayoshi Yoshida. Over the years, she also worked as a postdoctoral researcher in the Institute of Chemistry at UNESP and in the Department of Chemistry at UFSCar. In 2013, she was appointed Visiting Scientist at the University of Manchester. Her research interests involve isolation and stereostructural determination of natural products mainly through chiroptical methods associated with quantum-mechanical calculations.

Alessandra L. Valverde

Alessandra L. Valverde is an Associate Professor in the Institute of Chemistry at Fluminense Federal University, Brazil. She received a BSc in Industrial Chemistry (1993) and a MSc in Organic Chemistry (1996) from Fluminense Federal University, Brazil, and her PhD (1999) degree in Science from Federal University of Rio de Janeiro. Over the years, she also worked as P&D Researcher at FIOCRUZ (1999–2004) and as a postdoc in the Department of Chemistry at Federal University of São Carlos in 2017. She supervises postdoctoral, doctoral, master's and undergraduate students. Her research interests involve isolation and stereostructural determination of bioactive natural products.

may trigger responses in far more diverse biological contexts. As a result, humans have been making use of nature's vast chemical biodiversity for thousands of years in religious ceremonies, in producing pleasure, and in curing various diseases.[2] The medicinal potential of natural products can be better appreciated upon inspection of the number of approved drug molecules over the last 40 years that are either unmodified natural products or are derived or inspired in secondary metabolites.[3] In the area of cancer, for example, natural products were involved in almost 65% of the therapeutic agents approved between 1981 and 2019. All this potential, however, comes with a high price tag. Nature's intricate biosynthetic machinery associated with post-biosynthetic modifications/rearrangements[4] gives rise to complex structural scaffolds with varying stereochemical outcomes, including enantiomeric purity, depending on the producing organism.[5–8] Tackling stereochemical complexity is not a trivial task and, although quantum chemical calculations of NMR chemical shifts have become a great ally for the correct assignment of the structure and relative configurations of natural products,[9] the structural and physicochemical similarities between enantiomers make their differentiation particularly challenging. As a result, an increasing number of absolute configuration reassignments of secondary metabolites have been reported in the literature over the last decade.[10]

Absolute configuration assignment

The most established method for absolute configuration assignment is single crystal X-ray diffraction.[11] Nevertheless, it requires quality single crystals, which are commonly not attainable for secondary metabolites. Even when crystals are obtained, the Flack parameter[12] and/or the standard uncertainty are frequently outside the acceptable range, especially given the common lack of information about the compounds' enantiomeric purity.[6,11]

Nuclear magnetic resonance (NMR) methods are the primary source of structural information for natural product chemists.[13] Stereochemical information is commonly obtained from scalar couplings and nuclear Overhauser effect (NOE) experiments, nevertheless, such properties are identical for enantiomers, rendering NMR insensitive to chirality in isotropic media. As a result, most of the absolute configuration assignments by NMR involve the use of chiral derivatizing or solvating agents.[14]

Chiroptical methods, which originate from the interaction of a chiral non-racemic compound with circularly polarized electromagnetic radiation, are naturally sensitive to chirality and allow the stereochemical investigation of natural products directly in solution, without requiring either single crystals or derivatizations, in most cases. The main chiroptical methods are optical rotation (OR), its wavelength-dependent version, optical rotatory dispersion (ORD), electronic circular dichroism (ECD), vibrational circular dichroism (VCD), and Raman optical activity (ROA).[15] In the field of natural products, the application of OR and ECD to secondary metabolites has an important historical precedence over other methods.[16,17] Most of these applications, however, involve empirical spectral correlations between structurally related molecules. OR represents simply a signed number, whose magnitude reflects the optical purity of

Laurence A. Nafie

Laurence A. Nafie received his PhD from the University of Oregon in 1973, and from 1973 to 1975 he was a postdoctoral associate at the University of Southern California. In 1975 he moved to Syracuse University to establish a research program in VCD and Raman optical activity (ROA). In 1978 he carried out the first measurements of Fourier transform VCD, now the basis of all commercial VCD instrumentation. In 1988 he first measured scattered circular polarization (SCP) ROA now used in all commercially available ROA spectrometers. In 1996, he co-founded with Dr. Rina Dukor BioTools, Inc. to market instrumentation and services for VCD and ROA. In 2010 he became Editor-in-Chief of the Journal of Raman Spectroscopy, and in 2011 he published Vibrational Optical Activity: Principles and Applications by John Wiley & Sons. In 2013, he was named winner of the Pittsburgh Spectroscopy Award and in 2014 the Gold Medal Award of the Society of Applied Spectroscopy (SAS, NY Section). In 2019 he won the Chirality Medal. He is a Fellow (2008) and Honorary Member (2020) of the SAS and has over 320 publications and several patents.

João M. Batista Jr

João M. Batista Jr received a BSc in Pharmaceutical Sciences (2007) and a PhD in Chemistry (2012) from UNESP, Brazil. During 2009–2010 he was appointed Visiting Research Scholar at Syracuse University, USA. He then worked as a postdoctoral fellow at UNESP (2012–2015) with a period as Visiting Scientist at the University of Manchester (2012–2013). In 2015, he joined UFSCar, Brazil, to lead the first Vibrational Optical Activity research group in South America. Currently, he works as an assistant professor of chemistry at UNIFESP, in São José dos Campos, Brazil. His research involves stereochemical studies of small molecules and macromolecules using chiroptical methods and quantum-chemical calculations.

the sample. Nevertheless, no structural information is available from OR measurements and both the sign and magnitude of this chiroptical property may change upon varying experimental parameters, such as the solvent, concentration, and temperature. In the case of ECD, even though it is accompanied by the corresponding UV-vis absorbance spectrum, the small number of broad bands intrinsic to UV spectroscopy reduces its discriminative stereochemical power. As a consequence, the OR and ECD properties of structurally related molecules with the same absolute configuration may be significantly different or even opposite. This makes the empirical correlations mentioned above very risky, which can easily lead to misassignments.[18–22] VCD and ROA, on the other hand, circumvent most of the limitations described for OR and ECD since they are based on the structurally richer vibrational spectroscopic techniques IR and Raman, respectively. Current best practice guidelines recommend the use of computational methods to interpret both electronic and vibrational chiroptical experimental properties.[23]

Total synthesis is also an important tool to assign the structure and absolute configuration of complex natural products.[24] Stereoselective total synthesis, however, is a very time consuming and specialized procedure, and, at the end of the day, the absolute configuration assignment is performed by comparison of the spectral data (NMR, OR, and CD) of the natural product with that of the synthetic compound.[25,26]

Given the advantages of vibrational chiroptical spectroscopy over other techniques, herein, special attention will be paid to the use of VCD to assign the absolute configuration of secondary metabolites from different sources over the last decade. Although the FDA has recently recognized VCD as an acceptable method for assignment of absolute stereochemistry leading to its broader use both in academia and industry,[27] its application by the natural product community is still limited. In the following sections, further details about VCD will be provided along with best practices for stereochemical assignments and representative application examples.

Vibrational circular dichroism (VCD)

2024 marks the 50th anniversary of the first report of vibrational circular dichroism (VCD) spectra, which were recorded for neat 2,2,2-trifluoro-1-phenyl ethanol in 1974.[28] The discovery of VCD was confirmed shortly after in 1975 using the same molecule with the extension of the spectral range to include the OH stretching region.[29] Instrumental advancements then allowed VCD to be recorded in the mid-IR fingerprint region,[30] greatly improving its stereochemical discriminative power. This latter feature also triggered the successful longstanding relationship between VCD and natural products, especially monoterpenes. The enantiomers of α-pinene and camphor are used as validation standards for the sign and intensity calibration of VCD spectrometers.[31]

VCD is defined as the difference in absorbance by a chiral molecule for left- and right circularly polarized infrared (IR) radiation as described in eqn (1), where A_L and A_R represent absorbance for left- and right-circularly polarized radiation, respectively, and $(\bar{\nu})$ is the wavenumber frequency of the radiation. VCD can also be described in terms of molar absorptivity $(\Delta\varepsilon)$ by dividing the absorbance A by the product of the concentration in mol L^{-1} and the path length in cm.

$$\Delta A(\bar{\nu}) = A_L(\bar{\nu}) - A_R(\bar{\nu}) \quad (1)$$

As the circularly polarized components are themselves chiral, their differential interaction with enantioenriched or pure chiral secondary metabolites represents a manifestation of diastereomeric discrimination, making VCD a naturally chiral sensitive technique (as are other forms of chiroptical spectroscopy).[32] VCD can be considered the extension of conventional CD to the IR region of the electromagnetic spectrum, where molecular vibrational transitions occur. Since virtually any chemical bond may be considered a chromophore in the IR, a vast range of different molecular scaffolds can be directly analysed by VCD, in contrast to ECD which requires the presence of appropriate UV-vis chromophores in the target molecules. Another important feature of VCD is its sensitivity to the conformational dynamics in solution. Due to the timescale of a vibrational transition being significantly shorter than that of a conformational transition at room temperature ($\sim 10^{-15}$ s *vs.* $\sim 10^{-12}$ s),[33] the final VCD spectra carry contributions of as many conformers as possible that are present in a given solvent, according to their Boltzmann populations (weighted average). Such sensitivity is also observed for other chiroptical methods, nevertheless, since VCD is recorded in the mid-IR region (900–1800 cm^{-1}), it benefits from the wealth of structural information inherent to IR spectroscopy. As a result, different sources of chirality (centre, axis, and plane) may be probed simultaneously in a target molecule using IR/VCD.[34,35] On the other hand, the ratio between the size of the chromophore and the wavelength of incident radiation for VCD spectroscopy is smaller than that of UV-based CD, leading to intensities up to two orders of magnitude smaller. Consequently, VCD requires larger amounts of samples and longer measurement times when compared to ECD (see the next section).

VCD instrumentation is based on transmission FT-IR spectrometers which are modified to include optical elements that convert linearly polarized light into circularly polarized light (Fig. 1).[36] The main optical element is a photoelastic modulator (PEM) composed of a ZnSe crystal that can generate circularly polarized light components by means of quarter-wave retardations of linearly polarized incident light at frequencies between 37 and 50 kHz. This combined with an appropriate detector (*e.g.* nitrogen cooled MCT detector) allows IR and VCD spectra to be collected simultaneously. Manufacturers like BioTools Inc., Bruker, and Jasco offer either standalone FT-VCD instrumentation or accessories to existing FT-IR spectrometers. In

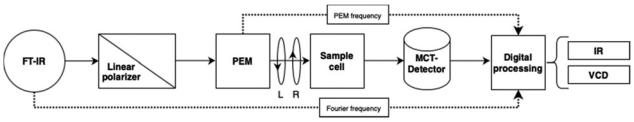

Fig. 1 Block diagram of a conventional VCD instrument. Reproduced from ref. 36.

contrast to the longstanding availability of (spectro)polarimeters and ECD spectrometers, the first commercially available FT-VCD spectrometer (BioTools Chiral*IR*) reached the market only in 1997, contributing to its less frequent use in academia and industry alike. Since its first development, a few advancements have been made to VCD instrumentation, the most significant of these include the use of dual-source for better signal-to-noise ratio (S/N), digital time-sampling replacing the use of lock-in amplifiers, and dual-PEM for improved baseline and real-time removal of birefringence artifacts.

VCD-based absolute configuration assignment

The classic methodology for the assignment of absolute configurations by means of VCD spectroscopy involves the comparison of experimental IR and VCD spectra with those simulated using density functional theory (DFT) methods. The apparent simplicity of this approach, though, hides important pitfalls that need to be considered. This section will present an overview of the main steps necessary for reliable VCD stereochemical assignments, which is summarized in Scheme 1. It is not intended, however, to be exhaustive and will be focused on solution-state measurements only. Applications and points of attention for measurements and simulations of solid-state VCD can be found elsewhere.[37–40] Solid sampling includes mainly mulls, films, and pellets. Currently, it is not possible to record ATR-based VCD spectra.

The requirements for a reliable VCD measurement are the same as those observed for liquid-state FT-IR. First, an appropriate solvent capable of dissolving the sample at concentrations of approximately 0.01–0.5 M is selected. Although rather concentrated solutions are used for IR and VCD measurements, the solvent is still the dominant component of the solution. As the solvent itself absorbs IR radiation, deuterated versions are used to avoid the interference of solvent absorbing bands that can reduce the sample IR signal at the detector. By replacing H with D, the reduced mass of the vibrating atoms changes, which shifts the solvent band vibrational frequencies to lower wavenumbers. The use of deuterated solvents is not mandatory, but it results in a much wider spectroscopic window in the fingerprint region. The most commonly used solvents are chloroform-d_1 ($CDCl_3$), acetonitrile-d_3 (ACN-d_3), methanol-d_4 (CD_3OD) and dimethylsulfoxide-d_6 (DMSO-d_6). Non-hydrogenated solvents such as carbon tetrachloride (CCl_4) and carbon disulfide (CS_2) may also be used. The use of protic deuterated solvents may lead to isotopic exchanges in the sample. This may be beneficial as in the case of glycosylated (ox-)anthrones in methanol-d_4 solution, in which isotopic exchange of the sugar moieties revealed spectral markers for the C10 absolute configuration. It was possible since the H/D exchange shifted the OH-related sugar vibrations into the range of the solvent absorbance, thus reducing the overlap with vibrational bands originating from the aglycone.[41] On the other hand, H/D exchange can also lead to the inversion of the sign of some VCD bands, resulting in almost mirror image spectral relationships for molecules with the same absolute configuration as revealed for caffeic acid ester derivatives using DFT calculations.[42] Therefore, in the case of polar natural products studied in protic deuterated solvents, different possibilities of isotopic exchange need to be considered. Ideally, a combination of VCD and isotopic-exchange-insensitive ECD is recommended for unambiguous assignments of absolute configuration. Sample cells of BaF_2 windows with path lengths ranging from 50–200 μm (for non-aqueous solutions) are the most frequently used for absolute configuration determinations. For measurement of aqueous (D_2O) or partially aqueous solutions, sample cells with CaF_2 windows and path lengths of 5–50 μm are required. Water is the most challenging solvent for VCD analysis. Sample concentration and path length are then adjusted to obtain IR bands in the mid-IR region within 0.1–0.9 absorption units. This condition may require the measurement of different regions of the spectrum separately. From a practical standpoint, the minimum amount of sample required for VCD analysis of small-molecule natural products is 3–5 mg. This may be an important bottleneck as some classes of natural products are produced in very small amounts. It is noteworthy, however, that VCD is a non-destructive technique, and the sample is commonly fully recovered after the measurement. IR and VCD spectra are collected simultaneously with a spectral resolution usually in the range of 4–8 cm^{-1}. Data are collected using blocks of variable time lengths (or a variable number of scans), which are averaged to yield the final spectra. The typical collection time of a VCD spectrum with a good S/N ratio varies from 1 to 12 h, or even longer depending on sample flexibility and the amount available. Finally, the VCD spectrum is baseline corrected either by taking the half difference of the VCD spectra of both enantiomers (recommended option) or by subtraction of the VCD spectrum of the corresponding racemate. These options also allow for the subtraction of occurring absorption artifacts; however, enantiomers or racemates are commonly not available for secondary metabolites. Alternatively, subtraction of the VCD spectrum recorded for the solvent under similar conditions may be used.

IR and VCD spectral simulations are predominantly performed at the DFT level using commercial software packages

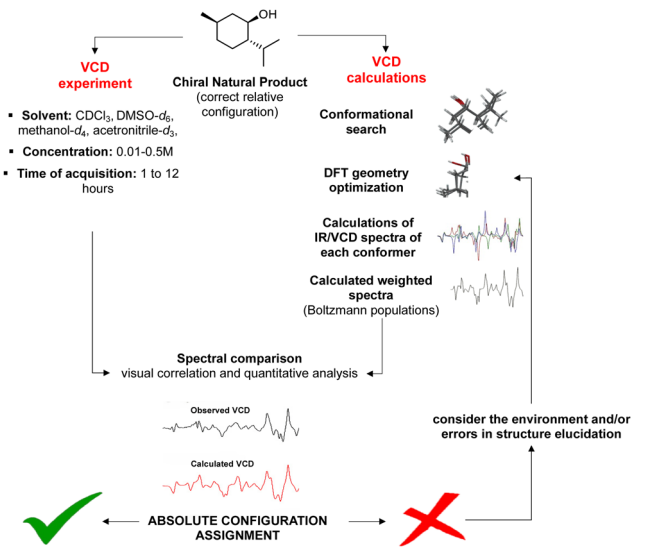

Scheme 1 General procedure for VCD-based stereochemical assignment. See the text for details.

such as Gaussian, Turbomole, ADF, ORCA, and Schrödinger. IR and VCD intensities are proportional to the dipole and rotational strengths, respectively. The dipole strength (D) is calculated as the square of the electric dipole transition moment vector (μ) of a vibrational normal mode, while the rotational strength (R) is obtained as the scalar product of the electric (μ) and magnetic (m) dipole moment vectors (eqn (2) and (3)), where 0 and 1 are the wavefunctions of ground and excited states, respectively.

$$D_{01} = |\langle 0|\mu|1\rangle|^2 \quad (2)$$

$$R_{01} = \mathrm{Im}\{\langle 0|\mu|1\rangle\cdot\langle 1|m|0\rangle\} = |\mu|\cdot|m|\cdot\cos\xi \quad (3)$$

Based on eqn (2) and (3), D is always positive, while R can be either positive or negative, depending on the absolute value of both vectors as well as their relative orientations (ξ).

Nevertheless, calculating VCD properties for a given molecule is the last step in a series of calculations. It is important to mention that chiroptical spectroscopy is ideal for discriminating enantiomers. Thus, before any calculation is performed, the relative configuration of molecules containing more than one stereocentre must be unambiguously determined. To that end, 1D and 2D-NMR spectroscopy assisted by quantum chemical calculations of ^{1}H and ^{13}C chemical shifts is the recommended protocol. Probability analysis, such as that performed with DP4+,[43] greatly improves the diastereoisomeric discriminative power of NMR calculations. If no relative configuration is known beforehand, the next steps described below must be performed for all possible diastereoisomers. It's noteworthy that chiroptical property calculations are not necessary for enantiomers, in which case, only one enantiomeric configuration needs to be selected arbitrarily. The VCD spectrum of the opposite enantiomer is generated simply by multiplying the calculated VCD intensity by −1.

Given the sensitivity of IR and VCD to different conformations, as described earlier, one of the most important steps is the correct identification of all conformers possibly present in a given solvent at the working temperature. This is particularly important since for flexible molecules, individual conformers may result in oppositely signed VCD bands, leading to their net intensity reduction. Conformational searches can be performed at the molecular mechanics (MM) force field level using either systematic search or Monte Carlo algorithms, as well as by means of meta-dynamics and MD methods.[44] In the case of MM, energy windows of roughly 10–20 kcal mol^{-1} are recommended to avoid overlooking potentially important conformers. Once the possible conformers are identified, they are subject to geometry optimization steps at the DFT level.

IR and VCD simulations must then be performed on optimized structures and at the same level of theory used for geometry optimization steps. The minimum model chemistry for VCD is B3LYP/6-31G(d), which performs well even for large molecules provided all significant conformers are correctly identified.[45] Other important hybrid functionals for VCD calculations include the dispersion corrected B3LYP-D3, B3PW91 and ωB97XD, combined with basis sets such as 6-311G(d,p), cc-pVDZ, DGDZVP, and TZVP. Sulfone containing molecules greatly benefit from simulations using the 6-311G(3df,2dp) basis (or equivalent Dunning and Ahlrichs variants) combined either with B3LYP or B3PW91 functionals.[46] IR and VCD frequency calculations of individual conformers also afford thermodynamic data, such as zero point correct electronic energies and Gibbs free energies. The energies of individual conformers are then used to create Boltzmann averaged IR and VCD spectra to be compared to the experiment. Only conformers contributing with more than 2% of the total Boltzmann distribution (relative energies typically $\leq$1.7 kcal mol^{-1}) are commonly considered. The Boltzmann averaged IR and VCD theoretical spectra are generated commonly using Lorentzian bands of half width at half maximum (HWHM) of 6–8 cm^{-1}. Frequency scaling factors (0.96–0.99) are frequently used to account for experimental anharmonicities not considered in the harmonic approximation used in standard vibrational frequency analysis. Recently, VCD anharmonic frequency calculations[47] have been implemented in commercial software packages. The VCD spectrum is then plotted above the IR spectrum in stack mode, on the same wavenumber frequency scale, to facilitate the correlation between absorbance and VCD bands, since any VCD band must have a corresponding IR band.

To determine the absolute configuration of a natural product molecule using VCD, the experimental IR and VCD spectra are compared to the spectra calculated for an arbitrarily chosen configuration. If the simulated absorption frequencies, relative intensities, and band signs (VCD) match those observed experimentally, the absolute configuration chosen for the calculation is assigned to the target molecule. If the simulated absorption frequencies and relative intensities match the experiment but the signs are reversed, then the configuration selected for the calculations corresponds to the enantiomer of the natural product in question. The qualitative level of agreement between experimental and calculated spectra is assessed visually in most cases. In order to avoid user bias and increase confidence in VCD-based assignments, methods for quantitative analysis of the level of agreement between experimental and calculated IR/VCD have been developed.[48–53] If significant discrepancies are observed between calculations and experiment, some scenarios must be considered, including incorrect structure, incorrect relative configuration, incorrect conformer populations, and strong solvent effects. Given that structure and relative configurations are unambiguously secured, some approaches may be used to improve theoretical simulations.

Conformer populations are based on DFT-predicted energies, which are prone to inaccuracies, especially considering entropic contributions to Gibbs free energies. This is particularly critical for conformers forming strong intra- and intermolecular hydrogen bonds. Creating spectra using simple averages of the lowest-energy conformers identified within a slightly expanded energy window ($\sim$3 kcal mol^{-1}) may be beneficial to double check a given assignment. Another option is the use of genetic algorithms that optimize the Boltzmann populations of a given conformational ensemble within a specified range of uncertainty.[45,54] Solvent effects, on the other

hand, may be accounted for using different methods. The simplest and most commonly used methods are continuum solvation models, which consider the molecule as inserted in a continuum medium of the dielectric constant of the solvent being modelled (molecular cavity).[55] Since no explicit solvent molecules are considered, they are referred to as implicit solvation. Common implicit solvation models include the polarizable continuum model (PCM) and the conductor-like screening model (COSMO). In the case of highly coordinating solvents such as methanol, dimethyl sulfoxide, and acetonitrile implicit solvation may not be sufficient. In such cases, different approaches to include explicit solvent molecules may be used. Microsolvation is the most commonly used method where a few solvent molecules are carefully placed around organic functionalities capable of engaging in H-bond interactions (solute–solvent clusters). These solvent molecules are treated quantum chemically, which increases the computational cost of the simulation but at the same time better represents the solvent environment and its influence in both conformational equilibria and spectral features.[56] Other cluster-generating methods include top-down approaches based on MD simulations,[57] or more recent bottom-up processes such as quantum cluster growth.[58] Regarding MD methods, snapshots of the simulations are commonly taken at regular time intervals and subject to quantum chemical calculations. If the number of solvent molecules becomes prohibitive to be treated quantum chemically, two-layer (or larger) methods may be employed, such as QM/MM.[59,60] More recent efforts have led to DFT MD methods[61] which, although more accurate than static methods, are still very demanding of computational power and limited to very small chiral molecules. One final simulation procedure involves the VCD study of carboxylic acids in apolar solvents. Since $CDCl_3$ is by far the most used solvent to study secondary metabolites, carboxylic acids tend to dimerize under these conditions, clearly impacting their IR and VCD properties. The presence of carboxylic acid dimers in solution can be easily simulated by including a molecule of a simple carboxylic acid, such as formic acid, properly oriented to interact with the target molecule by means of a double H-bond pattern.[62] Geometry optimization and frequency calculations are then performed at the DFT level for the molecular complex. Merten *et al.*[63] have recently proposed the use of 7-azaindole during the experiment to avoid the formation of carboxylic homodimers in $CDCl_3$ and, consequently, the need for the dimer simulation, as described above.

VCD and natural products

Over the last 25 years the use of VCD to assign absolute stereochemistry of natural products has been reviewed several times.[16,17,64–66] Interestingly, back in 2000 a single application example was reported, the Scolytidae insect pheromone frontalin.[16,67] Ever since then, hundreds of compounds have been investigated by means of VCD and DFT calculations. In this section, an overview of the growing application of VCD to natural product chemistry will be provided along with representative application examples.

To properly describe the evolution of VCD applied to natural products, we have searched the main literature databases to find absolute configuration assignments using VCD as the main method. The search covered the period from 1975 to early 2024 and included the following keywords: ''VCD or vibrational circular dichroism'' and ''absolute configuration'' and ''natural product or secondary metabolite''. This search of course was not meant to be exhaustive, and we anticipate many papers to be left out based on the keywords used. Despite the many contributions of monoterpenes to the development of VCD instrumentation and calculations, the only examples considered were those of monoterpenes that had their stereochemistry unambiguously assigned by VCD. Many manuscripts dealing with IR and VCD spectra of monoterpenes of known absolute configurations were not included. A total of 235 papers were found over this time period and within the search criteria used (see ESI†). It was only after 2005 that the application of VCD to stereochemical investigations of secondary metabolites started to gain traction. This observation makes sense considering that the first commercial VCD spectrometer would reach the market only in 1997. From 2010 onwards a steady growth in the number of yearly reports could be observed, reaching its maximum in 2019, when the numbers started to drop, possibly due to the worldwide impact of the COVID-19 pandemic (Fig. 2). Despite the encouraging number of papers over the years, it is noteworthy that half of the reports come from only four research groups, namely, Pedro Joseph-Nathan's (Cinvestav, Mexico, 59), the authors of the current highlight article (36), Kenji Monde's (Hokkaido University, Japan, 12) and Prasad Polavarapu's (Vanderbilt University, USA, 11). Prof. Joseph-Nathan, who sadly passed away in 2022, was the most prolific researcher on the application of VCD to natural products, studying a variety of secondary metabolites of different classes. His legacy is survived by his research group and former students. Nevertheless, except for Joseph-Nathan's, none of the groups mentioned above has classic natural product chemistry as the main research area. It is, therefore, important to attract more researchers to the VOA field, especially given the advantages of VCD over the other techniques available, as discussed above.

Application examples

This section will present selected examples published over the last five years that demonstrate the power of VCD to solve stereochemical problems of different classes of secondary metabolites. As the first example, the case of the bicyclo[3.2.1]octane neolignan nectamazin A (**1**) will be presented.[68] (+)-nectamazin A was previously reported in 2009 from *Nectandra amazonum* Nees. (Lauraceae) and had its absolute configuration assigned as 7*R*,8*S*,3′*S*,4′*R*,5′*S* by comparison of its OR and ECD properties with those of structurally related compounds. Our phytochemical investigations on *Ocotea aciphylla* (Lauraceae) led to the isolation of (+)-nectamazin A. Interestingly, nectamazin A presented a positive specific rotation in $CHCl_3$, while negative values were observed in CH_3OH solution, emphasizing the risks of comparing chiroptical data. Since the stereochemistry of (+)-nectamazin A had been assigned based on risky empirical

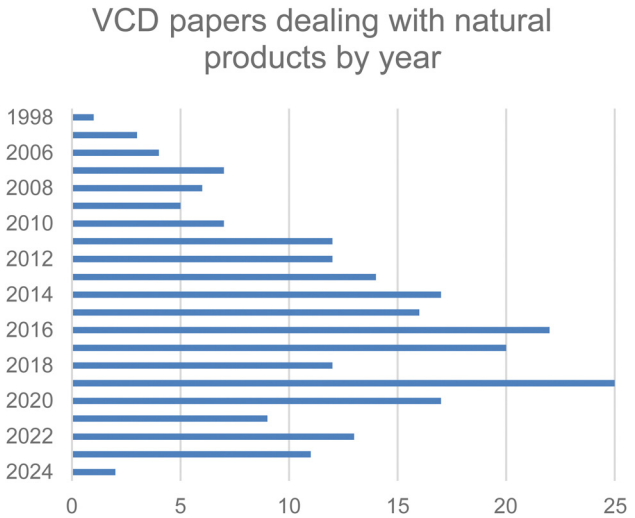

Fig. 2 Number of reports of VCD-based stereochemical assignments of natural products over the years. 2024 encompasses Jan–Mar.

correlations, VCD experiments and calculations were performed for nectamazin A. For the calculations, the absolute configuration previously described in 2009 was arbitrarily chosen. Upon comparing the IR and VCD experimental data with those calculated at the DFT level, a mirror image relationship was observed for the VCD spectra indicating that the absolute configuration chosen for the calculations was actually enantiomeric to that observed experimentally. The absolute configuration of (+)-nectamazin A was therefore reassigned as 7*S*,8*R*,3′*R*,4′*S*,5′*R* (Fig. 3).

A second representative example involves the case of the bisindane marine natural products papuamine (**2**) and haliclonadiamine (**3**), isolated from the sponge *Haliclona* sp (Fig. 4).[54] Previous studies based on total synthesis, X-ray crystallography, and ECD spectroscopy on **2** and **3** led to conflicting results regarding their relative stereochemical structures.[69] Therefore, VCD was used to provide definite proof of their absolute configurations. Nevertheless, the high flexibility of the putative compounds prevented the accurate use of the standard protocol based on Boltzmann factors calculated with DFT methods, since uncertainties of at least 5 kcal mol^{-1} for the computed relative energies were identified. This stereochemical challenge was circumvented by employing a combination of genetic and hierarchical clustering machine learning algorithms. Besides providing the best agreement between experimental and calculated data, this method also assesses the level of agreement between the experimental data and the incorrect enantiomer, thus yielding more reliable assignments. This approach was applied to both VCD and ECD spectral analyses of the marine natural products. VCD results (Fig. 4) led to the unambiguous assignment of the absolute configurations of **2** and **3** as 1*R*,3*S*,8*R*,9*S*,14*S*,15*R*,20*S*,22*R* and 1*S*,3*R*,8*S*,9*R*,14*R*,15*S*,20*R*,22*R*, respectively, confirming the more recent assignment by X-ray crystallography.[69] ECD, however, was found to generate ambiguous results, which could not be addressed either by the standard method or the genetic and machine learning algorithms. The superior performance of VCD over ECD is explained

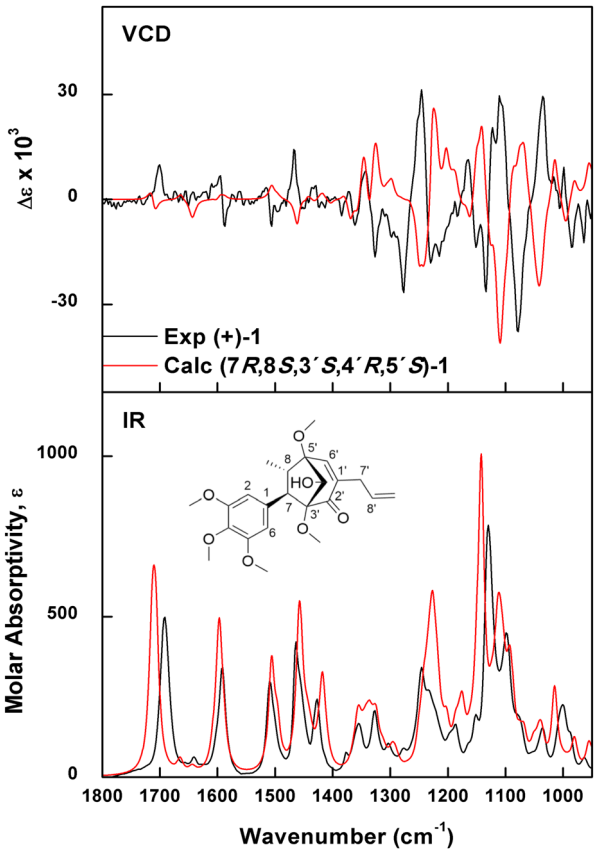

Fig. 3 Comparison of experimental and calculated IR and VCD spectra of (+)-nectamazin A (**1**) isolated from *O. aciphylla*. The structure depicts the absolute configuration originally assigned and arbitrarily chosen for the calculations. Experiment in $CDCl_3$ and calculations at the B3PW91/PCM($CHCl_3$)/6-311G(d,p) level. Reprinted with permission from ref. 68. Copyright (2024) Elsevier.

by the larger number of bands present in the IR fingerprint region in contrast to the significantly fewer bands observed in the UV spectrum. Since the experimental ECD spectra of **2** and **3** presented a single negative band, no reliable conclusion could be drawn as the individual conformers of these flexible molecules provide predominantly mirror-image ECD spectra.

Another interesting example is that of the polyketide natural product (−)-enterocin (**4**) (Fig. 5).[70] This compound was originally reported in 1976 from cultures of two strains of *Streptomyces* and had its structure proposed based on the X-ray crystallographic analysis of *m*-bromobenzoyl enterocin dihydrate.[71] All further isolations of natural (−)-**4** assumed the stereostructure depicted in the original manuscript as its absolute structure, even though the chemical absolute configuration was not determined. Only recently, synthetic efforts combined with VCD experiments and calculations finally revealed that the absolute configuration of (−)-**4** was indeed the opposite of that originally assumed (Fig. 5). Therefore, the absolute configuration of the complex polyketide (−)-**4** was assigned as 2*R*,3*R*,4*R*,5*S*,6*S*,8S,9*R*. These results have far-reaching consequences for biosynthetic studies of structurally related molecules and evidence the risks of error propagations in (stereo)structural assignments of natural products.

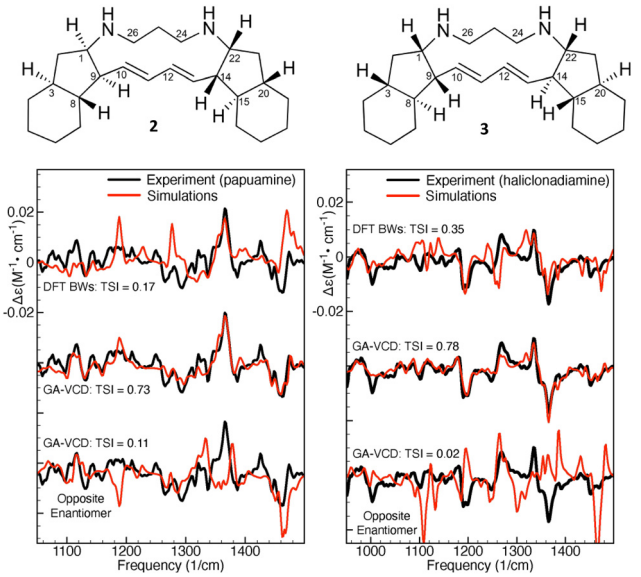

Fig. 4 (top) Structures of papuamine (**2**) and haliclonadiamine (**3**). (bottom) Comparison of experimental and calculated VCD spectra of **2** and **3** for the correct and opposite enantiomers using both the standard DFT Boltzmann-weighted (BW) and the genetic algorithm (GA) approaches. TSI represents the Tanimoto similarity index. Reprinted with permission from ref. 54.

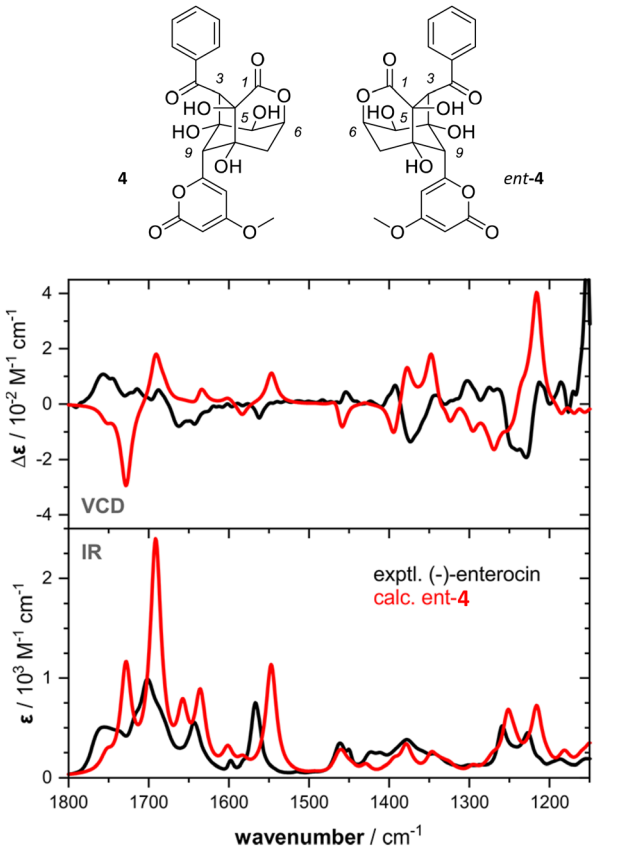

Fig. 5 (Top) Structures of (−)-enterocin (**4**) and *ent*-**4**, originally considered the correct structure. (Bottom) Comparison of experimental IR and VCD spectra of (−)-enterocin with the calculated spectra for *ent*-**4**. Experiment in CD_3OD and calculations at the B3LYP/IEFPCM(MeOH)/6-31 + G(2d,p) level. Reprinted with permission from ref. 70. Copyright (2022) American Chemical Society.

The following example deals with the biogenetically hybrid prenyl indole alkaloid giluterrin (**5**) (Fig. 6) produced by *Aspergillus terreus* P63 grown in solid medium of rolled oats.[34] This compound contains two stereocenters (C2″ and C3″) connecting the fused dihydrofuran and dihydropyrrolidine rings, whose relative configurations are readily assigned by NMR spectroscopy. In addition, a substituted indolic ring at C-5 may give rise to atropo-diastereomers as revealed by the potential energy barrier calculated for the full rotation around the dihedral angle C4–C5–C3′–C2′ ($\sim$70 kcal mol^{-1}). In order to unambiguously assign the absolute configuration of the different chiral elements present in (−)-**5**, VCD experiments and DFT calculations were performed. The very good correlation between experimental and theoretical data allowed the assignment of (−)-**5** as 5*P*,2″*R*,3″*R*. Interestingly, comparisons between the calculated IR and VCD spectra obtained for the atropoisomers at C5 revealed distinct contributions of central and axial chirality to the VCD spectrum (Fig. 6). The lower wavenumber region of the spectrum was dominated by vibrational modes involving the stereogenic centers C2″ and C3″, while the region above 1400 cm^{-1} reflected the configuration of the atropoisomeric portion of the molecule. These results demonstrate the power of VCD to probe simultaneously different elements of chirality within the same molecule.

In line with the assignment of different chiral elements, the next example deals with the simultaneous determination of different hierarchical levels of chirality, namely, central chirality and secondary structure. The target molecules were cyclic plant peptides known as orbitides. VCD analysis of linear counterparts also revealed the conformational restrictions induced by the backbone head-to-tail cyclization. The study[72] was focused on synthetic versions (all-L and all-D) of the orbitide pohlianin A (**6**) (Fig. 7), originally isolated from *Jatropha pohliana*. The original report[73] of all-L natural pohlianin A identified a single mean conformation for the peptide in DMSO-d_6 solution by means of NMR spectroscopy, which was described as containing a conventional type I β-turn at Val_4-Leu_5, and a β-bulge motif with a type VIa β-turn around Tyr_7-Pro_1, with *cis*-tyrosyl-proline amide bond. The IR and VCD study initially confirmed the opposite absolute configurations of the amino acids in all-L and all-D **6**, which was evident by their mirror-image VCD spectra (Fig. 7), while presenting nearly identical IR. The comparison between experimental and calculated VCD data then allowed a detailed conformational analysis of the peptide. Besides identifying the originally reported conformation, VCD and DFT results led to the description of two additional significantly populated conformers with distinct secondary structures in ACN-d_3 solution (Fig. 7). Interestingly, the mean conformation described in DMSO-d_6 was not the lowest-energy conformer identified by VCD. The additional secondary structure elements described for pohlianin A included three classic γ-turns, two involving Gly_3 and one Leu_6. VCD was also sensitive to the stacking of the pyrrolidine ring of proline and the aromatic ring of tyrosine. Recent reinvestigations of the experimental and calculated VCD spectra of pohlianin A

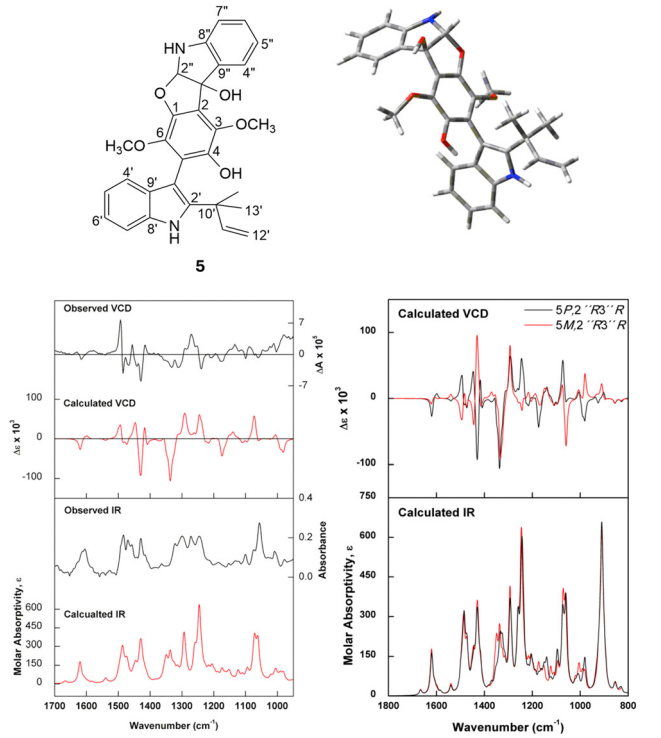

Fig. 6 (Top) Planar structure of giluterrin (**5**) and the lowest-energy conformer identified for (5*P*,2″*R*,3″*R*)-**5**. (Bottom left) Comparison of experimental IR and VCD spectra of (−)-giluterrin with the calculated spectra for (5*P*,2″*R*,3″*R*)-**5**. (Bottom right) Comparison of calculated IR and VCD spectra (5*M*,2″*R*,3″*R*)- and (5*P*,2″*R*,3″*R*)-**5**. Experiment in $CDCl_3$ and calculations at the B3LYP/6-31G(d) level. Reprinted with permission from ref. 34. Copyright (2019) Elsevier.

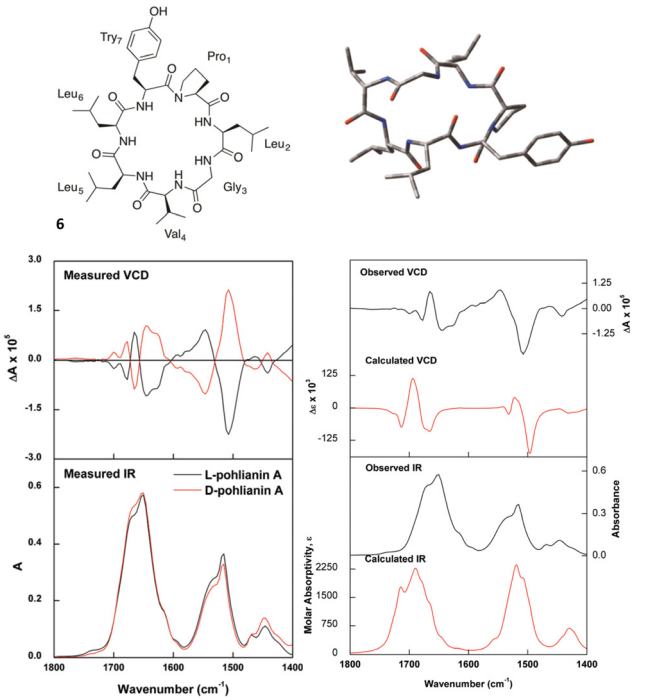

Fig. 7 (top) Structures of all-L pohlianin A (**6**) and the lowest-energy conformation identified. (bottom left) Comparison of experimental IR and VCD spectra of all-L and all-D **6**. (bottom right) Comparison of experimental and calculated IR and VCD spectra of all-L **6**. Experiment in ACN-d_3 and calculations at the B3PW91/PCM(ACN)/cc-pVDZ level. Reprinted with permission from ref. 72. Copyright (2022) the Royal Society of Chemistry.

aided by artificial intelligence algoritms[45] led to the identification of other secondary structure elements, enhancing even further the conformational sensitivity of VCD for cyclic peptides. These included a larger share of β-strand residues, including Leu_2, Leu_6 and Tyr_7; β-turns of type II′ (Gly_3-Val_4) and type VIa2 (Tyr_7-Pro_1); inverse γ-turns (Leu_2 and Leu_5); and a twisted macrocyclic shape stabilized by an intramolecular hydrogen bond. It is important to mention, however, that in spite of the demonstrated potential of VCD for simultaneous configurational and conformational analysis of plant cyclic peptides, some studies have recently indicated that VCD may not be able to assign the absolute configuration of heterochiral cyclic peptides containing three or more stereocenters.[74]

The next example involves the phytotoxic neocassane diterpene neocassa-12(17),15-dien-3-one (**7**) (Fig. 8), isolated from *Eragrostis plana*.[75] Compound **7** was isolated along with four other biosynthetic related molecules. Although for two of them X-ray crystallography provided the relative configuration, single crystals were not obtainable for (+)-**7**. Additionally, compound **7** presented a particular chiral center, for which the relative configuration could not be unambiguously assigned by NMR spectroscopy. Therefore, IR and VCD experiments and calculations were carried out. The DFT calculations were carried out for both diastereomers possible at C13, namely, (5*R*,8*S*,9*S*,10*R*,13*R*)- and (5*R*,8*S*,9*S*,10*R*,13*S*)-**7**. Although both C13 epimers of **7** presented very similar IR and VCD spectra, a band at 1255 cm^{-1} was oppositely signed in their calculated spectra (Fig. 8). The band in question arises from sp^3-CH and CH_2 deformation modes involving most of the molecular framework and only the VCD spectra simulated for the *R*-configured epimer matched the experimental spectrum. Therefore, the absolute configuration of (+)-**7** was assigned as 5*R*,8*S*,9*S*,10*R*,13*R*. As this assignment was based on the sign of a single band, quantitative analysis of the agreement between experimental and calculated data was carried out using the confidence level algorithm.[50] Additionally, qualitative and quantitative analyses of the vibrational dissymmetric factor (VDF)[51] were also performed. VDF is the ratio of VCD to IR spectra and has the advantage of being concentration-independent in addition to avoiding over- or underestimation of predicted band intensities. All similarity results largely favored the 13*R* configuration of (+)-**7**.

The final example demonstrates the enhanced sensitivity of VCD to small structural and stereochemical changes in the macrolide antibiotics clarithromycin (**8**) and erythromycin (**9**) (Fig. 9).[76] Clarithromycin is a semi-synthetic methoxylated derivative of the natural product erythromycin, produced by bacteria such as *Saccharopolyspora erythraea*. These represent very challenging cases for VCD investigation due to high flexibility and the presence of multiple chiral centers. As expected, their IR spectra were virtually indistinguishable. Despite that, the VCD spectra of **8** and **9** presented band patterns that clearly

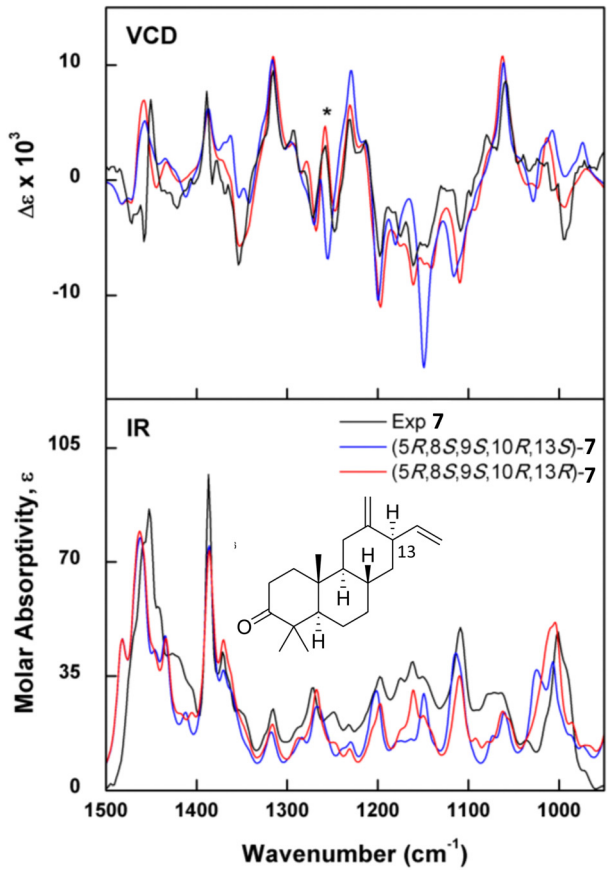

Fig. 8 Comparison of experimental IR and VCD spectra of (+)-neocassa-12(17),15-dien-3-one (**7**) with calculated data for both epimers at C13. The asterisk indicates the discriminative VCD band at 1255 cm^{-1}. Experiment in $CDCl_3$ and calculations at the B3PW91/6-311G(d,p) level. Reprinted with permission from ref. 75. Copyright (2020) American Chemical Society.

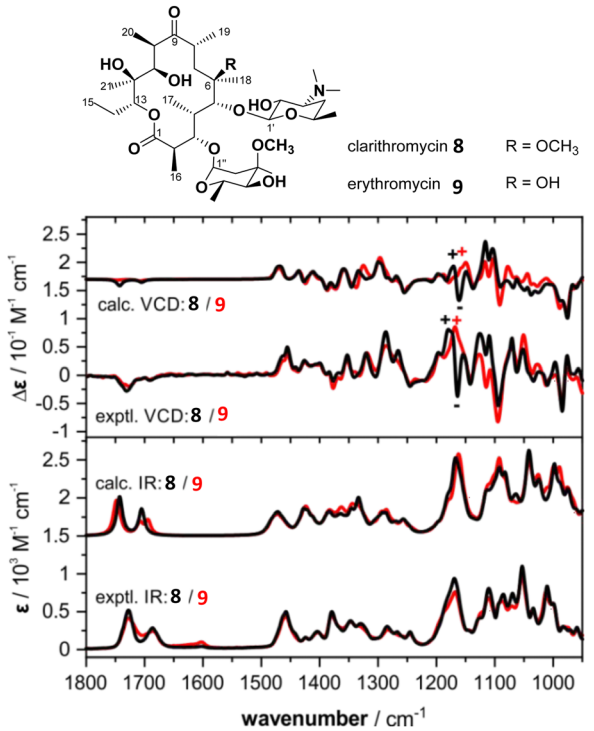

Fig. 9 (top) Structures of clarithromycin (**8**) and erythromycin (**9**). (bottom) Comparison of experimental and calculated IR and VCD spectra of the macrolides **8** and **9**. Experiment in $CDCl_3$ and calculations at the B3LYP/IEFPCM($CHCl_3$)/6-31G(2d,p) level. Reprinted with permission from ref. 76. Copyright (2020) the Royal Society of Chemistry.

differentiate them. The bands between 1200–1150 cm^{-1} presented a (+/−) pattern for **8**, while an all-positive signature was observed for **9** (Fig. 9), which were correctly reproduced by the DFT calculations. The underlying vibrational modes of the above-mentioned band patterns involve C1–O stretchings coupled to C–H bendings at C2 and C13 for the positive VCD bands found at 1178 cm^{-1} for **8** and 1168 cm^{-1} for **9**. The characteristic negative VCD band at 1164 cm^{-1} observed for **8**, on the other hand, contains strong contributions of the C–O–C stretching vibration of the methoxy group. This confirms the sensitivity of VCD to small structural changes in such complex structures, regardless of having the same absolute configuration at C6. Further investigations also revealed that the VCD spectra of these compounds are dominated by vibrations of the macrocycle, with weak contributions from the sugar moieties. Such enhanced discriminatory power of VCD for the stereochemistry of the macrocyclic moiety was supported using DFT calculations for epimeric structures of **8** involving C6, C8, C12 and C13. The relative configuration of these chiral centers could not be determined based on NMR *J*-coupling constants. IR and VCD, however, showed important spectral variation for the epimers in the region of 1250–1150 cm^{-1}, suggesting that the experimental differentiation of these epimers should be possible. In a follow-up study,[77] the same authors reported an unprecedented effect of a single residual water molecule in $CDCl_3$ solution for the stabilization of an extended hydrogen bonding network in azithromycin, as revealed by VCD.

Conclusions

VCD is one the most powerful stereochemical tools available to determine simultaneously the absolute configuration and conformer population in solution, being applicable at various stages of the drug discovery pipeline.[78] The examples shown in the previous section clearly demonstrate its potential to solve complex cases; however, even after 50 years since its first report, it is still unknown to a large part of the natural product chemistry community worldwide. Among the main reasons for its reduced use in natural product-oriented research programs are the amount of sample required, the still limited availability of FT-VCD spectrometers in most universities and industries, along with the need for DFT calculations to interpret experimental data. The former may be tackled by the development of micro-sampling accessories,[79] resulting in up to one order magnitude reduction in sample volume. The latter is expected to improve in the near future with the development of dedicated software suites combining all steps, from conformational searches to calculations of chiroptical properties and

comparison with experiment, in a single simulation. Over the last fifteen years, a tremendous increase in computational power has been observed, with supercomputer facilities becoming available to researchers worldwide.

Even those without access to such facilities can nowadays assemble computer clusters of different sizes that allow the simulation of multiple multi-core calculations simultaneously. Strategies such as conformational rigidification have also been put forward, facilitating the analysis of flexible molecules and reducing the computational expenses required for optimization and CD calculations.[80–82] In some cases, as with acetonide formation in polyhydroxylated molecules,[83] calculations may be avoided altogether. Other promising approaches, which involve the search and validation of IR and VCD spectral markers, either by visual inspection or machine learning methods, may also lead to the identification and stereochemical assignments of chiral molecules even in mixtures and without further DFT calculations.[84] With the increased availability of accessible methods to interpret experimental spectra, combined with smaller sample requirements, more natural product researchers will feel encouraged and confident to use VCD routinely. Such increased interest in VCD would consequently lead to a higher demand for dedicated instrumentation, taking it from niche laboratories to multiuser analytical centres, as is the case for ECD.

Data availability

No primary research results, software or code have been included and no new data were generated or analysed as part of this review.

Conflicts of interest

There are no conflicts to declare.

Acknowledgements

Fundação de Amparo à Pesquisa do Estado de São Paulo – FAPESP (grant# 2023/12475-5) and Fundação de Amparo à Pesquisa do Estado do Rio de Janeiro – FAPERJ (grant# E-26/202.761/2023) are acknowledged for funding.

Notes and references

1 A. L. Demain and A. Fang, in *Advances in Biochemical Engineering/Biotechnology - History of Modern Biotechnology I.*, ed. A. Fiechter, Springer, Berlin, 2000, vol. 69, ch. 1, pp. 1–39.
2 V. De Luca, V. Salim, S. M. Atsumi and F. Yu, *Science*, 2012, **336**, 1658.
3 D. J. Newman and G. M. Cragg, *J. Nat. Prod.*, 2020, **83**, 770.
4 P. M. Dewick, *Medicinal natural products: a biosynthetic approach*, Wiley, 2009.
5 J. M. Finefield, D. H. Sherman, M. Kreitman and R. M. Williams, *Angew. Chem., Int. Ed.*, 2012, **51**, 4802.
6 A. N. L. Batista, F. M. Santos Jr., J. M. Batista Jr. and Q. B. Cass, *Molecules*, 2018, **23**, 492.
7 A. J. E. Novak and D. Trauner, *Trends Chem.*, 2020, **2**, 1052.
8 G. T. M. Bitchagno, V.-A. Nchiozem-Ngnitedem, D. Melchert and S. A. Fobofou, *Nat. Rev. Chem.*, 2022, **6**, 806.
9 M. O. Marcarino, M. M. Zanardi, S. Cicetti and A. M. Sarotti, *Acc. Chem. Res.*, 2020, **53**, 1922.
10 A. N. L. Batista, B. R. P. Angrisani, M. E. D. Lima, S. M. P. Silva, V. H. Schettini, H. A. Chagas, F. M. Santos Jr., J. M. Batista Jr. and A. L. Valverde, *J. Braz. Chem. Soc.*, 2021, **32**, 1499.
11 A. Valentín-Pérez, P. Rosa, E. A. Hillard and M. Giorgi, *Chirality*, 2022, **34**, 163.
12 H. D. Flack, *Acta Crystallogr., Sect. A: Found. Crystallogr.*, 1983, **39**, 876.
13 D. S. Wishart, Z. Sayeeda, Z. Budinski, A. Guo, B. L. Lee, M. Berjanskii, M. Rout, H. Peters, R. Dizon, R. Mah, C. Torres-Calzada, M. Hiebert-Giesbrecht, D. Varshavi, D. Varshavi, E. Oler, D. Allen, X. Cao, V. Gautam, A. Maras, E. F. Poynton, P. Tavangar, V. Yang, J. A. van Santen, R. Ghosh, S. Sarma, E. Knutson, V. Sullivan, A. M. Jystad, R. Renslow, L. W. Sumner, R. G. Linington and J. R. Cort, *Nucleic Acids Res.*, 2022, **50**, D665.
14 S. K. Mishra and N. Suryaprakash, *Tetrahedron: Asymmetry*, 2017, **28**, 1220.
15 F. M. Santos Jr. and J. M. Batista Jr., in *Chiral Separations and Stereochemical Elucidation*, ed. Q. B. Cass, M. E. Tiritan, J. M. Batista Jr. and J. C. Barreiro, John Wiley & Sons, Hoboken, 1st edn, 2023, ch. 14, pp. 551–591.
16 S. Allenmark, *Nat. Prod. Rep.*, 2000, **17**, 145.
17 A. Mándi and T. Kurtán, *Nat. Prod. Rep.*, 2019, **36**, 889.
18 A. Nakahashi, Y. Yaguchi, N. Miura, M. Emura and K. Monde, *J. Nat. Prod.*, 2011, **74**, 707.
19 J. M. Batista Jr., B. Wang, M. V. Castelli, E. W. Blanch and S. N. López, *Tetrahedron Lett.*, 2015, **56**, 6142.
20 H. Zhou, L. Li, C. Wu, T. Kurtán, A. Mándi, Y. Liu, Q. Gu, T. Zhu, P. Guo and D. Li, *J. Nat. Prod.*, 2016, **79**, 1783.
21 D. Padula and G. Pescitelli, *Molecules*, 2018, **23**, 128.
22 T.-M. Lv, R. Guo, B.-H. Yang, P. Zhao, B. Lin, X.-X. Huang and S.-J. Song, *Phytochemistry*, 2024, **222**, 114067.
23 H. Zhu, Y. Wang and L. A. Nafie, *Front. Nat. Prod.*, 2022, **1**, 1086897.
24 K. C. Nicolaou and S. Rigol, *Nat. Prod. Rep.*, 2020, **37**, 1404.
25 F. Della-Fellice, R. A. Pilli and A. M. Sarotti, *J. Braz. Chem. Soc.*, 2018, **29**, 1041.
26 M. Dandawate, R. Choudhury, G. R. Krishna and S. Reddy, *J. Nat. Prod.*, 2023, **86**, 1878.
27 S. S. Wesolowski and D. E. Pivonka, *Bioorg. Med. Chem. Lett.*, 2013, **23**, 4019.
28 G. Holzwarth, E. C. Hsu, H. S. Mosher, T. R. Faulkner and A. Moscowitz, *J. Am. Chem. Soc.*, 1974, **96**, 251.
29 L. A. Nafie, J. C. Cheng and P. J. Stephens, *J. Am. Chem. Soc.*, 1975, **97**, 3842; L. A. Nafie, T. A. Keiderling and P. J. Stephens, *J. Am. Chem. Soc.*, 1976, **98**, 2715.
30 E. D. Lipp, C. G. Zimba and L. A. Nafie, *Chem. Phys. Lett.*, 1982, **90**, 1.
31 United State Pharmacopeia, 39-NF34, 2016, ch. 782.
32 N. Berova, L. Di Bari and G. Pescitelli, *Chem. Soc. Rev.*, 2007, **36**, 914.
33 G. Pescitelli, L. Di Bari and N. Berova, *Chem. Soc. Rev.*, 2011, **40**, 4603.
34 J. R. Gubiani, M. C. S. Oliveira, R. A. R. Nepomuceno, M. J. Camargo, W. S. Garcez, A. R. Biz, M. A. Soares, A. R. Araujo, V. S. Bolzani, H. C. F. Lisboa, P. T. Sousa Jr., L. G. Vasconcelos, T. A. N. Ribeiro, J. M. Oliveira, T. P. Banzato, C. A. Lima, G. B. Longato, J. M. Batista Jr., R. G. S. Berlinck and H. L. Teles, *Phytochem. Lett.*, 2019, **32**, 162.
35 M. Fusè, G. Mazzeo, S. Abbate, R. Ruzziconi, J. Bloino and G. Longhi, *Chirality*, 2024, **36**, e23649.
36 J. Bogaerts, R. Aerts, T. Vermeyen, C. Johannessen, W. Herrebout and J. M. Batista Jr., *Pharmaceuticals*, 2021, **14**, 877.
37 C. Merten, T. Kowalik and A. Hartwig, *Appl. Spectrosc.*, 2008, **62**, 901.
38 J. E. Rode, K. Lyczko, K. Kosińska, J. Matalińska, J. Dyniewicz, A. Misicka, J. C. Dobrowolski and P. F. J. Lipiński, *Spectrochim. Acta, Part A*, 2022, **269**, 120761.
39 S. Jähnigen, *Angew. Chem., Int. Ed.*, 2023, **62**, e202303595.
40 K. Dobšíková, T. Taušová, P. Fagan, N. Paškanová, M. Kuchař, J. Čejka and V. Setnička, *Spectrochim. Acta, Part A*, 2024, **305**, 123486.
41 P. Demarque, D. R. Pinho, N. P. Lopes and C. Merten, *Chirality*, 2018, **30**, 432.
42 G. V. Ccana-Ccapatinta, B. L. Sampaio, F. M. Santos Jr., J. M. Batista Jr. and F. B. Costa, *Tetrahedron: Asymmetry*, 2017, **28**, 1823.
43 M. O. Marcarino, S. Cicetti, M. M. Zanardi and A. M. Sarotti, *Nat. Prod. Rep.*, 2022, **39**, 58.

44 S. Grimme, *J. Chem. Theory Comput.*, 2019, **15**, 2847.
45 J. M. Batista Jr. and V. P. Nicu, *Phys. Chem. Chem. Phys.*, 2023, **25**, 22111.
46 K. Scholten, E. Engelage and C. Merten, *Phys. Chem. Chem. Phys.*, 2020, **22**, 27979.
47 M. Fusè, G. Longhi, G. Mazzeo, S. Stranges, F. Leonelli, G. Aquila, E. Bodo, B. Brunetti, C. Bicchi, C. Cagliero, J. Bloino and S. Abbate, *J. Phys. Chem. A*, 2022, **126**, 6719.
48 P. J. Stephens, F. J. Devlin and J.-J. Pan, *Chirality*, 2008, **20**, 643.
49 J. Shen, C. Zhu, S. Reiling and R. Vaz, *Spectrochim. Acta, Part A*, 2010, **76**, 418.
50 E. Debie, E. De Gussem, R. K. Dukor, W. Herrebout, L. A. Nafie and P. Bultinck, *Chem. Phys. Chem.*, 2011, **12**, 1542.
51 P. L. Polavarapu and C. L. Covington, *Chirality*, 2014, **26**, 539.
52 J. Vandenbussche, P. Bultinck, A. K. Przybył and W. A. Herrebout, *J. Chem. Theory Comput.*, 2013, **9**, 5504.
53 L. Böselt, D. Sidler, T. Kittelmann, J. Stohner, D. Zindel, T. Wagner and S. Riniker, *J. Chem. Inf. Model.*, 2019, **59**, 1826.
54 G. Marton, M. A. J. Koenis, H.-B. Liu, C. A. Bewley, W. J. Buma and V. P. Nicu, *Angew. Chem., Int. Ed.*, 2023, **62**, e202307053.
55 B. Mennucci, *WIREs Comput. Mol. Sci.*, 2012, **2**, 386.
56 C. Merten, *Phys. Chem. Chem. Phys.*, 2023, **25**, 29404.
57 M. Spasovová, J. Kapitán, Š. Jílek, M. S. P. Kkadan, J. Klener, N. S. Lynn Jr., V. Kopecký Jr., V. Baumruk and V. Profant, *Spectrochim. Acta, Part A*, 2024, **313**, 124119.
58 A. R. Puente and P. L. Polavarapu, *Spectrochim. Acta, Part A*, 2024, **303**, 123231.
59 T. Giovannini, M. Olszòwka and C. Cappelli, *J. Chem. Theory Comput.*, 2016, **12**, 5483.
60 S. Ghidinelli, S. Abbate, J. Koshoubu, Y. Araki, T. Wada and G. Longhi, *J. Phys. Chem. B*, 2020, **124**, 4512.
61 D. R. Galimberti, *J. Chem. Theory Comput.*, 2022, **18**, 6217.
62 J. M. Batista Jr., A. N. L. Batista, D. Rinaldo, W. Vilegas, Q. B. Cass, V. S. Bolzani, M. J. Kato, S. N. Lopez, M. Furlan and L. A. Nafie, *Tetrahedron: Asymmetry*, 2010, **21**, 2402.
63 C. Grassin, E. Santoro and C. Merten, *Chem. Commun.*, 2022, **58**, 11527.
64 L. A. Nafie, *Nat. Prod. Commun.*, 2008, **3**, 451.
65 J. M. Batista Jr., E. W. Blanch and V. S. Bolzani, *Nat. Prod. Rep.*, 2015, **32**, 1280.
66 P. L. Polavarapu and E. Santoro, *Nat. Prod. Rep.*, 2020, **37**, 1661.
67 C. S. Ashvar, P. J. Stephens, T. Eggimann and H. Wieser, *Tetrahedron: Asymmetry*, 1998, **9**, 1107.
68 A. N. L. Batista, C. H. T. Santos, A. C. F. Albuquerque, F. M. Santos Jr., F. R. Garcez and J. M. Batista Jr., *Spectrochim. Acta, Part A*, 2024, **304**, 123283.
69 H.-B. Liu, G. H. Imler, K. K. Baldridge, R. D. O'Connor, J. S. Siegel, J. R. Deschamps and C. A. Bewley, *J. Am. Chem. Soc.*, 2020, **142**, 2755.
70 L. Koser, C. Grassin, C. Merten and T. Bach, *Org. Lett.*, 2022, **24**, 6903.
71 Y. Tokuma, N. Miyairi and Y. Morimoto, *J. Antibiot.*, 1976, **29**, 1114.
72 M. A. S. Yokomichi, H. R. L. Silva, L. E. V. N. Brandao, E. F. Vicente and J. M. Batista Jr., *Org. Biomol. Chem.*, 2022, **20**, 1306.
73 C. Auvin-Guette, C. Baraguey, A. Blond, H. S. Xavier, J.-L. Pousset and B. Bodo, *Tetrahedron*, 1999, **55**, 11495.
74 K. D. R. Eikas, M. Krupova, T. Kristoffresen, M. T. P. Beerepoot and K. Ruud, *Phys. Chem. Chem. Phys.*, 2023, **25**, 14520.
75 A. P. P. K. Hendges, E. F. dos Santos, S. D. Teixeira, F. S. Santana, M. M. Trezzi, A. N. L. Batista, J. M. Batista, Jr., V. A. de Lima, F. A. Marques and B. H. L. N. S. Maia, *J. Nat. Prod.*, 2020, **83**, 3511.
76 D. P. Demarque, S. Heinrich, F. Schulz and C. Merten, *Chem. Commum.*, 2020, **56**, 10926.
77 D. P. Demarque, M. Kemper and C. Merten, *Chem. Commum.*, 2021, **57**, 4031.
78 A. McGown, J. Nafie, M. Otayfah, S. Hassel-Hart, G. J. Tizzard, S. J. Coles, R. Banks, G. P. Marsh, H. J. Maple, G. E. Kostakis, I. P. Silvestri, P. Colbon and J. Spencer, *RSC Chem. Biol.*, 2023, **4**, 716.
79 X. Lu, H. Li, J. W. Nafie, T. Pazderka, M. Pazderková, R. K. Dukor and L. A. Nafie, *Appl. Spectrosc.*, 2017, **71**, 1117.
80 F. J. Devlin, P. J. Stephens and P. Besse, *J. Org. Chem.*, 2005, **70**, 2980.
81 A. Mandí, M. M. M. Swamy, T. Taniguchi, M. Anetai and K. Monde, *Chirality*, 2016, **28**, 453.
82 A. Nakahashi, A. K. C. Siddegowda, M. A. S. Hammam, S. G. B. Gowda, Y. Murai and K. Monde, *Org. Lett.*, 2016, **18**, 2327.
83 F. Passareli, A. N. L. Batista, A. J. Cavalheiro, W. A. Herrebout and J. M. Batista Jr., *Phys. Chem. Chem. Phys.*, 2016, **18**, 30903.
84 T. Vermeyen, A. N. L. Batista, A. L. Valverde, W. Herrebout and J. M. Batista Jr., *Phys. Chem. Chem. Phys.*, 2023, **25**, 13825.

